ChemComm

COMMUNICATION

View Article Online
View Journal | View Issue

Cite this: *Chem. Commun.*, 2026, **62**, 5514

Received 20th January 2026,
Accepted 17th February 2026

DOI: 10.1039/d6cc00195e

rsc.li/chemcomm

Peptide structure and silver ion affinity: influence on the formation of α-helices upon metal binding

Alexandre Bianchi and Katharina M. Fromm *

Metal ion binding is essential for many critical life-sustaining protein functions. To clarify Ag^+ resistance, we studied model peptides based on the SilE protein. By focusing on a specific sequence of SilE known to form α-helices and mutants thereof, we discovered trends in the α-helical structure induced by Ag^+.

Silver, in its ionic or nanoparticle form, exhibits antimicrobial properties.[1–3] While the precise mechanisms underlying this phenomenon remain to be fully elucidated, research has shown that treating bacteria with silver results in the interference of silver ions with biomolecules, leading to their alteration.[4,5] This includes alteration of the cell membrane,[6,7] condensation of DNA by intercalation into base pairs,[7,8] protein damage (*e.g.*, mismetallation, liganding thiol groups (–SH), or iron–sulfur destabilization),[9–11] and direct or indirect production of reactive oxygen species (ROS).[7,8,10] Consequently, these factors culminate in the inhibition of cell respiration, ultimately leading to the demise of the bacteria.[4,5]

However, some Gram-negative bacteria, such as *Salmonella typhimurium*, display a remarkable degree of tolerance to the antimicrobial effect of silver, which exceeds that observed in other bacterial strains.[12–15] This phenomenon can be attributed to the expression of a silver efflux pump, which is known as the Sil system (Fig. 1).[12] This system consists of eight proteins that work together to actively export Ag^+ out of the bacteria.

In more detail, the periplasmic sensor SilS detects the arrival of Ag^+ and subsequently activates the response regulator SilR, which in turn induces the transcription of the SilPFABC operon.[12] Among these components, it has been suggested that SilP functions as a P-type ATPase.[17] This type of pump is known to facilitate the selective transport of ions across biological membranes. SilP is hypothesized to initiate the transfer of Ag^+ from the cytoplasm to SilF in the periplasm. However, further investigation is necessary to ascertain its precise structural characteristics and functional role.[18] SilF, located in the periplasm, functions as a chaperone protein and binds only one Ag^+ *via* coordination with four specific amino acid (aa) residues in its sequence.[19] The SilABC complex is a tripartite efflux pump responsible for the transport of Ag^+ from the periplasm or the cytoplasmic space to the extracellular environment.[12]

Among the Sil proteins, SilE seems to play a distinct role: initially reported to bind five Ag^+, later studies suggest the capacity to accommodate up to eight Ag^+, acting as a "silver sponge" at high concentration.[12,20–22] Only SilABC and SilE were shown to confer silver tolerance in bacteria.[16]

A previous study conducted within our research group on the B2 sequence excerpt from SilE (Fig. 2a), which can be generalized as $HX_2MX_3HX_2M$, showed that this peptide forms an α-helix upon silver ion binding. The separation of histidine (His, H) and methionine (Met, M) residues by two aa, as in the two HX_2M binding sites, positions the coordinating ligands on the same side of the α-helix. This configuration enables the linear coordination of each Ag^+ ion (Fig. 2b).[24]

In order to gain a deeper understanding of the manner in which the secondary structure exerts its influence on the

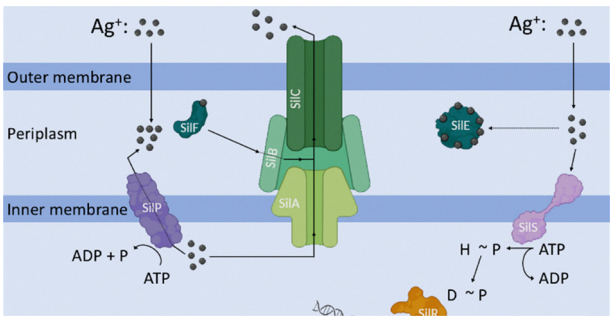

Fig. 1 The Sil system, a silver efflux pump in *Salmonella typhimurium*, consists of eight proteins working in concert to ensure high Ag^+ tolerance. The SilS (sensor) and SilR (regulator) control gene expression; the SilP (pump) and SilF (chaperone) transfer Ag^+; the SilABC forms the main efflux pump; and the SilE sequesters Ag^+ at high concentrations. (Adapted from Randall *et al.*[16] using BioRender.)

Univ. Fribourg, Department of Chemistry and National Center of Competence in Research Bio-inspired Materials, Chemin du Musée 9, 1700, Fribourg, Switzerland. E-mail: katharina.fromm@unifr.ch

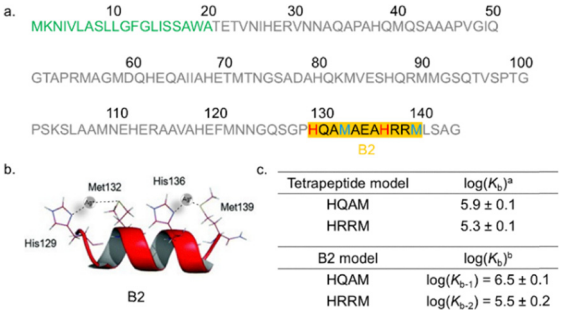

Fig. 2 (a) The SilE protein sequence composed of 143 aa, with the twenty-first aa (green) functioning as the signal peptide.[23] The motif (underlined in black) studied by Chabert *et al.* served as the inspiration for this study on mutated peptides.[24] (b) The lowest energy NMR structure of the B2 model with Ag^+, as highlighted by Chabert *et al.*[24] (c) [a] Binding constant ($\log(K_b)$) of HQAM and HRRM tetrapeptides from ref. 18. [b] $\log(K_{b\text{-}1/2})$ of the B2 model determined in this study.

binding constant ($\log(K_b)$) of Ag^+, a series of systematic mutations derived from the B2 sequence in SilE were synthesized and analyzed (see Table 1).

All synthesized sequences were protected on the N-terminal by acetylation and on the C-terminal by amidation (see SI). The presence of the product was confirmed by electrospray ionization mass spectrometry (ESI-MS) (Fig. S11–S18, SI). The B2 mutations were applied in specific regions, including in one or both HX_2M binding motifs, in the three-residue linker connecting them, or in the entire segment encompassing both motifs and the linker. This systematic approach was designed to elucidate the individual contributions of each structural element to the overall binding properties of the peptide. This strategy was guided by our previous findings on tetrapeptide models, which established that the HX_2H motif exhibited a significantly higher affinity for Ag^+ than the MX_2M motif or the hybrid motifs HX_2M and MX_2H.[25] Also based on these results, we selected glutamine (Gln, Q), alanine (Ala, A) and lysine (Lys, K) for the mutations, as our previous study revealed that these three aa showed the strongest contrast in $\log(K_b)$ behaviour. Indeed, Gln and Ala yielded high $\log(K_b)$ values, while Lys led to lower ones.[25] By modulating the $\log(K_b)$ *via* targeted mutations, we aimed to understand how local sequence variations and secondary structure influence Ag^+ coordination, consistent with Chabert *et al.*'s ^{1}H NMR study of B2 peptide–Ag^+ interactions.[24]

To investigate changes in peptide secondary structure upon Ag^+ coordination, circular dichroism (CD) titration experiments were performed on the wild-type B2 peptide and its mutants (Fig. S20–S27, SI, Table 1). The secondary structure content was then estimated *via* the DichroWeb server with the CDSSTR algorithm (Fig. S20–S27, SI).[26–28]

These experiments highlighted several notable trends:

(1) In their native state, the studied peptides are predominantly disordered, exhibiting CD spectra characteristic of random coil conformations. The net charge (NC) of each peptide (calculated as the sum of Glu/E: [−1] and Arg/R and Lys/K: [+1] per residue at pH 7.4) varies between [−1] and [+4]. Most peptides with moderate positive NC [+1 or +2], such as the wild-type B2 [+1], are largely unstructured. However, mutants like M11-B2 [+1] and M15-B2 [+1] exhibit significant α-helicity in the absence of Ag^+, suggesting that specific motif compositions can sometimes override the effect of NC.

(2) Upon Ag^+ addition, most peptides exhibit a strongly increased α-helicity, suggesting that metal-induced folding is a prevalent phenomenon as previously documented in the

Table 1 Helicity and binding constants of the peptides at 25 °C. Helicity was determined from CD titrations with the use of $AgNO_3$ (0 to 20.0 eq.). Binding constants ($\log(K_{b\text{-}1/2})$) were measured by fluorimetry competition titration using the HEWM probe (1 eq.) in MOPS buffer (20 eq., pH 7.4–7.5) with the use of $AgNO_3$ (0 to 5.0 eq.)

Code	Model	Helicity without Ag^+ [%]	Helicity with Ag^+ (plateau) [%]	Ag^+ to reach plateau [eq.]	$\log(K_{b\text{-}1})$	$\log(K_{b\text{-}2})$
B2	HQAMAEAHRRM	18	78	4	6.5 ± 0.1	5.5 ± 0.2
M1-B2	HQAMAAAHRRM	3	76	4	6.0 ± 0.1	5.2 ± 0.2
M2-B2	HQQMAEAHRRM	8	80	4	6.4 ± 0.1	5.4 ± 0.1
M3-B2	HQAMAEAHKRM	7	80	4	6.3 ± 0.1	5.1 ± 0.2
M4-B2	HQQMAEAHKKM	3	74	4	6.3 ± 0.1	5.4 ± 0.1
M5-B2	HQAHAEAHRRM	2	70	8	6.5 ± 0.1	5.5 ± 0.2
M6-B2	HQQHAEAHRRM	3	71	8	6.6 ± 0.1	5.6 ± 0.2
M7-B2	HQAMAEAHRRH	22	71	8	6.4 ± 0.1	5.7 ± 0.1
M8-B2	HQAMAEAHKRH	16	68	8	6.2 ± 0.2	5.5 ± 0.2
M9-B2	HQAMAEAHQQH	5	49	4	6.4 ± 0.1	5.6 ± 0.2
M10-B2	HQAHAEAHRRH	4	37	12	6.5 ± 0.1	5.6 ± 0.1
M11-B2	MQAMAEAHRRM	53	76	2	6.3 ± 0.1	5.0 ± 0.2
M12-B2	MKKMAEAHRRM	3	72	8	5.8 ± 0.1	5.1 ± 0.2
M13-B2	HQAMAEAMRRM	49	76	2	6.3 ± 0.1	5.1 ± 0.1
M14-B2	HQAMAEAMKKM	25	73	2	6.2 ± 0.1	4.9 ± 0.2
M15-B2	MQAMAEAMRRM	69	75	Native	5.9 ± 0.1	5.0 ± 0.1
M16-B2	HQQHAEAHQQH	5	<20	—	6.8 ± 0.1	6.0 ± 0.1
M17-B2	MKKMAEAMKKM	<1	<20	—	5.6 ± 0.2	4.6 ± 0.2
M18-B2	MKKMAEAHQQH	<1	<20	—	6.3 ± 0.2	4.9 ± 0.2
M19-B2	HQQHAAAHQQH	<1	<20	—	6.6 ± 0.1	5.9 ± 0.1
M20-B2	MKKMAAAMKKM	<1	<20	—	5.6 ± 0.1	4.7 ± 0.2
M21-B2	MKKMAAAHQQH	4	<20	—	6.4 ± 0.1	5.8 ± 0.1

literature.[24,29] Peptides with moderate NC [+1], particularly those with minimal modifications relative to B2, exhibit efficient folding. Conversely, highly charged [+3 or +4] or negatively charged [−1] peptides exhibit a diminished or delayed folding response. This suggests that NC and charge distribution along the sequence modulate the efficiency of α-helix formation.

(3) Peptides containing two HX_2M motifs and differing from the wild-type sequence B2 by only one mutation (*e.g.*, B2 [+1], M1-B2 [+2], M2-B2 [+1], M3-B2 [+1], and M4-B2 [+1]) exhibit high α-helicity. Addition of up to four equivalents of Ag^+ leads to maximal folding, reaching a plateau of resp. 78%, 76%, 80%, 80%, and 74%. Here, the motif structure is the predominant factor in facilitating efficient folding, while NC plays a minor role, as peptides with slightly higher NC (*e.g.* M1-B2 [+2]) still exhibit near-maximal helicity. The two HX_2M motifs stabilize the $O_i \rightarrow N_{i+4}$ H-bond along the backbone, providing rigidity and enabling linear coordination of Ag^+ (Fig. 2b).

(4) Replacing one HX_2M motif with HX_2H, a change in behavior is observed. In mutants such as M5-B2 [+1], M6-B2 [+1], M7-B2 [+1], and M8-B2 [+1], a higher concentration of Ag^+ (up to eight equivalents) is required to reach a folding plateau. Moreover, the maximum α-helical content achieved is typically lower, resp. 70%, 71%, 71%, and 68%.

According to the HSAB theory, this phenomenon seems paradoxical, since Ag^+ has a higher affinity toward His than to Met.[25] However, this stronger and more rigid coordination with His reduces the conformational flexibility required for α-helix stabilization. Conversely, the more flexible and adaptable coordination with Met better accommodates the subtle structural adjustment necessary for efficient folding.

Electrostatics also seems to play a role. M5 to M8-B2 [+1] behave similarly, but M9-B2 [−1] folds earlier, reaching its plateau after four equivalents of Ag^+ with lower helicity (49%). This indicates that an imbalanced charge distribution can facilitate premature folding while impeding the complete stabilization of the α-helix.

(5) When both HX_2M motifs are replaced with HX_2H, as is in M10-B2 [+1], α-helix formation is severely compromised. The process of folding necessitates the presence of many equivalents of Ag^+; however, maximal helicity remains low (37%). This can be attributed to the peptide's sequence and backbone conformation no longer providing the necessary support for the stabilizing H-bond network essential for maintaining a stable α-helix. In this case, motif identity predominates over NC because the structure itself hinders efficient helix formation. ESI-MS analysis under Ag^+ excess conditions indicates a peptide : Ag^+ ratio of 1 : 2 (Fig. S19), similar to that observed by Chabert *et al.* for the B2 sequence.[24]

(6) Substituting one HX_2M motif with MX_2M, as shown by M11-B2 [+1], M12-B2 [+3], M13-B2 [+1], and M14-B2 [+1], exposed the interplay between the motif and NC. Peptides with a moderate charge [+1] rapidly reach high helicity (resp. 76%, 76%, and 73%) with two equivalents of Ag^+. Conversely, the highly positively charged peptide (M12-B2) requires eight equivalents of Ag^+, reaching slightly lower maximal helicity (72%). This comparison demonstrates that an excess of positive charge on the peptide requires more Ag^+, likely due to electrostatic repulsion, while peptides with moderate charge efficiently adopt an α-helical structure upon Ag^+ addition.

(7) As previously indicated, the peptide in which both HX_2M motifs are replaced by MX_2M, M15-B2 [+1], exhibits substantial α-helical structure even in its native, unbound state (69%). Ag^+ addition modestly increases helicity (75%), suggesting that this specific motif combination intrinsically promotes α-helix formation, largely independent of NC.

(8) Mutants M16-B2 to M21-B2 exhibit low α-helical content (<20%), which remains largely unaffected by Ag^+ addition. This indicates that these heavily mutated sequences are unable to adopt a stable α-helical structure and that Ag^+ binding does not induce significant folding.

In the second part of the study, $\log(K_{b\text{-}1/2})$ values for each model peptide (Table 1) were determined *via* fluorometric competition titration experiments (Fig. S28–S71, SI), following our previous methodology,[25] and validated using the HEWM probe ($\log(K_b) = 6.4 \pm 0.1$).[24] MOPS was used as the optimal buffer.[30] For the wild-type B2 peptide, stepwise coordination of two Ag^+ was observed, $\log(K_{b\text{-}1}) = 6.5 \pm 0.1$ and $\log(K_{b\text{-}2}) = 5.5 \pm 0.2$, reflecting high affinity in the full peptide context. In this case, $K_{b\text{-}1}$ = [Ag–Peptide]/[Ag]·[Peptide] and $K_{b\text{-}2}$ = [Ag_2–Peptide]/[Ag]·[Ag–Peptide]. Conversely, isolated tetrapeptide motifs (HQAM and HRRM) bind one Ag^+ with moderate affinity (resp. 5.9 ± 0.1 and 5.3 ± 0.1) (Fig. 2c), showing that the full B2 sequence enhances Ag^+ binding.

The analysis of $\log(K_{b\text{-}1/2})$ across the peptide series highlights that Ag^+ binding efficiency is modulated by the chemical nature of the donor residues, as well as sequence-dependent factors, including motif type, NC, and α-helicity propensity. The experimental values vary widely: the strongest peptides bind the first Ag^+ approx. 16 times and the second approx. 25 times more strongly than the weakest. His-rich peptides with HX_2H motifs, such as M16-B2 ($\log(K_{b\text{-}1}) = 6.8 \pm 0.1$ and $\log(K_{b\text{-}2}) = 6.0 \pm 0.1$), show the highest Ag^+ $\log(K_{b\text{-}1/2})$, due to the strong binding of Ag^+ to the His imidazole ring, with the epsilon nitrogen (N_ε) atom acting as the primary electron donor. Conversely, Met-rich sequences that contain MX_2M motifs, such as M17-B2 ($\log(K_{b\text{-}1}) = 5.6 \pm 0.2$ and $\log(K_{b\text{-}2}) = 4.6 \pm 0.2$), exhibit reduced affinity due to less optimal Ag^+ coordination *via* the delta sulfur (S_δ) atom. Peptides with mixed HX_2M motifs (*e.g.*, B2, M1-B2, M2-B2: $\log(K_{b\text{-}1})$ = 6.0–6.5 and $\log(K_{b\text{-}2})$ = 5.1–5.5) exhibit intermediate binding behavior, suggesting moderate but not maximal affinity due to the mixed donor types.

Beyond the composition of the motifs, the overall NC affects Ag^+ binding. Peptides with moderate positive charge [+1 or +2], such as B2, demonstrate efficient binding, whereas highly charged peptides whether positive (*e.g.*, M12-B2 [+3], $\log(K_{b\text{-}1}) = 5.8 \pm 0.1$ and $\log(K_{b\text{-}2}) = 5.1 \pm 0.2$) or negative (*e.g.*, M9-B2 [−1], $\log(K_{b\text{-}1}) = 6.4 \pm 0.1$ and $\log(K_{b\text{-}2}) = 5.6 \pm 0.2$), exhibit more variable or lower $\log(K_{b\text{-}1/2})$. This suggests that electrostatic repulsion or imbalance can disrupt Ag^+ coordination, even with favorable donor residues.

The observed charge-dependent trends are consistent with predominantly enthalpic effects, although entropic contributions

(*e.g.* counterion release, changes in conformational freedom) may also play a role. Similar enthalpy-entropy balance constraints have been observed for other metal ions (*e.g.*, Cu^{2+} or Zn^{2+}), suggesting that these principles may extend beyond Ag^+.[31–33] However, the specific balance of these principles depends on each metal's coordination chemistry.

In conclusion, the present study highlights the delicate equilibrium that is meticulously orchestrated by nature in the B2 peptide, wherein secondary structure stability and Ag^+ coordination are in equilibrium. A systematic analysis of a series of mutants was conducted to demonstrate that both motif identity and NC play a critical role in the efficiency of α-helix formation and Ag^+ binding. Concerning the motifs, the hierarchy of Ag^+ binding and helical stability is apparent. Peptides comprising two HX_2M motifs exemplify the optimal compromise, exhibiting high helicity while maintaining effective Ag^+ coordination. Substituting one HX_2M with HX_2H results in an increase in Ag^+ affinity; however, this substitution also leads to a reduction in the flexibility required for the stable formation of an α-helix. In contrast, peptides that contain two HX_2H motifs undergo a substantial disruption in folding. Met-rich peptides, as exemplified by M15-B2, exhibit significant intrinsic helicity yet exhibit comparatively diminished Ag^+ affinity. The presence of mixed motifs, such as $HX_2MX_3MX_2M$ or $MX_2MX_3HX_2M$, indicates an intermediate behavior that reflects a balance between structural rigidity and Ag^+ binding efficiency.

A comparison with our earlier tetrapeptide study reveals common trends: His consistently displays a higher affinity for Ag^+ than Met.[25] However, undecapeptides investigated in this study demonstrate higher binding constants ($10^{4.9}$ to $10^{6.8}$ *vs.* $10^{4.8}$–$10^{6.0}$).[25] A further notable distinction is that, in the vast majority of cases, undecapeptides exhibit helicity, whereas tetrapeptides are too short, thus allowing us to probe how secondary structure formation modulates Ag^+ coordination.

This study shows that nature finely tuned B2 to strike a balance between structural stability and functional Ag^+ binding, thus providing a sophisticated framework for understanding metal–protein interactions. This insight can guide the design of bioinspired peptides with controllable helicity and tailored metal-binding. Peptide engineering has been successfully applied to modulate structure and function. For instance, Smith *et al.* introduced metal-binding motifs into short peptides (10 aa) to stabilize α-helices *via* Zn^{2+} or Cu^{2+} coordination,[34] while Hadianamrei *et al.* designed short peptides (13 or 15 aa) with optimised sequence to enhance anticancer activity and minimize toxicity.[35]

Our research will continue on SilE to better understand the Ag^+ coordination, particularly why it adopts a helical structure upon Ag^+ binding. While this particular protein is of interest in the context of silver resistance, the overall concept of tuning the structural properties of proteins with metal ions is of major interest in understanding biological processes. Structure–property relationships in chemistry represent a fascinating area, and we aim to further contribute to this field.

K. M. F. provided the initial idea, won competitive funding, and supervised the entire project. A. B. performed the experiments. All authors contributed to writing and reviewing the final version and approved its submission.

Conflicts of interest

There are no conflicts to declare.

Data availability

Data supporting this article have been included as part of the supplementary information (SI). Supplementary information: experimental methods and data. See DOI: https://doi.org/10.1039/d6cc00195e.

Acknowledgements

The authors thank the University of Fribourg, Fribourg Center for Nanomaterials, Swiss National Science Foundation (Projects: 2000020_172777 and 2000020_204215) for generous support, and Dr Martin Spichty for the insightful conversation.

References

1 D. J. Barillo and D. E. Marx, *Burns*, 2014, **40**, S3.
2 S. Medici, M. Peana, V. M. Nurchi and M. A. Zoroddu, *J. Med. Chem.*, 2019, **62**, 5923.
3 W. Sim, R. T. Barnard, M. A. T. Blaskovich and Z. M. Ziora, *Antibiotics*, 2018, **7**, 93.
4 S. H. Lee and B. H. Jun, *Int. J. Mol. Sci.*, 2019, **20**, S3.
5 F. Barras, L. Aussel and B. Ezraty, *Antibiotics*, 2018, **7**, 1.
6 A. V. Domínguez, R. A. Algaba, A. M. Canturri, Á. R. Villodres and Y. Smani, *Antibiotics*, 2020, **9**, 36.
7 T. C. Dakal, A. Kumar, R. S. Majumdar and V. Yadav, *Front. Microbiol.*, 2016, **7**, 1831.
8 H. O. Khalifa, A. Oreiby, T. Mohammed, M. A. A. Abdelhamid, E. N. Sholkamy, H. Hashem and R. M. Fereig, *Front. Cell. Infect. Microbiol.*, 2025, **15**, 1599113.
9 E. Dube and G. E. Okuthe, *Microbiol. Res.*, 2025, **16**, 110.
10 J. R. Morones-Ramirez, J. A. Winkler, C. S. Spina and J. J. Collins, *Microbiol.*, 2013, **5**, 190.
11 C. Tambosi, R. Liotenberg, S. Bourbon, M.-L. Steunou, A.-S. Babot, M. Durand, A. Kebaili and N. Ouchane, *mBio*, 2018, **9**, 6.
12 S. Silver, *FEMS Microbiol. Rev.*, 2003, **27**, 341.
13 G. L. Mchugh, R. C. Moellering, C. C. Hopkins and M. N. Swartz, *Lancet*, 1975, **1**, 235.
14 A. Gupta, K. Matsui, J.-F. Lo and S. Silver, *Nat. Med.*, 1999, **5**, 183.
15 S. L. Percival, P. G. Bowler and D. Russell, *J. Hosp. Infect.*, 2005, **60**, 1.
16 C. P. Randall, A. Gupta, N. Jackson, D. Busse and A. J. O'Neill, *J. Antimicrob. Chemother.*, 2015, **70**, 1037.
17 S. Silver, A. Gupta, K. Matsui and J.-F. Lo, *Met.-Based Drugs*, 1999, **6**, 315.
18 J. S. Klein and O. Lewinson, *Metallomics*, 2011, **3**, 1098.
19 R. M. Lithgo, M. Hanževački, G. Harris, J. J. A. G. Kamps, E. Holden, T. M. Gianga, J. L. P. Benesch, C. M. Jäger, A. K. Croft, R. Hussain, J. L. Hobman, A. M. Orville, A. Quigley, S. B. Carr and D. J. Scott, *J. Biol. Chem.*, 2023, **299**, 105331.
20 Y. Monneau, C. Arrault, C. Duroux, M. Martin, F. Chirot, L. Mac Aleese, M. Girod, C. Comby-Zerbino, A. Hagège, O. Walker and M. Hologne, *Phys. Chem. Chem. Phys.*, 2022, **25**, 3061.
21 V. Chabert, M. Hologne, O. Sénèque, A. Crochet, O. Walker and K. M. Fromm, *Chem. Commun.*, 2017, **53**, 6105.
22 L. Babel, M. H. Nguyen, C. Mittelheisser, M. Martin, K. M. Fromm, O. Walker and M. Hologne, *Chem. Commun.*, 2021, **57**, 8726.
23 UniProtKB, https://www.uniprot.org/uniprot/Q9Z4N3#, (accessed 7th May 2025).
24 V. Chabert, M. Hologne, O. Sénèque, O. Walker and K. M. Fromm, *Chem. Commun.*, 2018, **54**, 10419.

25 A. Bianchi, F. Marquenet, L. Manciocchi, M. Spichty and K. M. Fromm, *Chem. Commun.*, 2025, **61**, 5309.
26 N. Sreerama, S. Y. Venyaminov and R. W. Woody, *Anal. Biochem.*, 2000, **287**, 243.
27 N. Sreerama and R. W. Woody, *Anal. Biochem.*, 2000, **287**, 252.
28 A. J. Miles, S. G. Ramalli and B. A. Wallace, *Protein Sci.*, 2022, **31**, 37.
29 F. E. C. Blanc, M. Hologne, M. Demontrond, H. Chermette and O. Walker, *J. Phys. Chem. Lett.*, 2025, DOI: 10.1021/acs.jpclett.6c00044.
30 L. Babel, S. Bonnet-Gómez and K. M. Fromm, *Chemistry*, 2020, **2**, 193.
31 C. Sacco, R. A. Skowronsky, S. Gade, J. M. Kenney and A. M. Spuches, *J. Biol. Inorg. Chem.*, 2012, **17**, 531.
32 M. J. Lachenmann, J. E. Ladbury, N. B. Phillips, N. Narayana, X. Qian and M. A. Weiss, *J. Mol. Biol.*, 2002, **316**, 969.
33 A. M. Rich, E. Bombarda, A. D. Schenk, P. E. Lee, E. H. Cox, A. M. Spuches, L. D. Hudson, B. Kieffer and D. E. Wilcox, *J. Am. Chem. Soc.*, 2012, **134**, 10405.
34 S. J. Smith, K. Du, R. J. Radford and F. Akif Tezcan, *Chem. Sci.*, 2013, **4**, 3740.
35 R. Hadianamrei, M. A. Tomeh, S. Brown, J. Wang and X. Zhao, *J. Colloid Interface Sci.*, 2022, **607**, 488.

